Resonant tunneling in zero-dimensional nanostructures

Garnett W. Bryant
McDonnell Douglas Research Laboratories, P.O. Box 516, Saint Louis, Missouri 63166-0516
(Received 22 August 1988)

Resonant tunneling through a semiconductor quantum nanostructure, consisting of laterally confined contact regions, barriers, and a laterally confined quantum well (quantum box), has been observed recently. Fine structure in the resonant tunneling has been attributed to the discrete density of states in the quantum box. We investigate two mechanisms to explain the fine structure in the quantum-box resonant tunneling (QBRT). In QBRT the carrier can tunnel through the structure without changing its lateral subband, just as the electron in normal resonant-tunneling tunnels without changing its lateral wave vector. However, the lateral states are discrete in QBRT, and resonant tunneling should occur at different applied biases for different subbands. The discrete density of lateral states produces one peak in the resonant tunneling current for each well state and occupied source-contact subband. We determine the conditions necessary to resolve structure that is due to the discrete lateral levels. Even when only one source-contact lateral subband is occupied, tunneling through other levels will occur if subband mixing at the interfaces, due to lateral wave-function mismatch at the interfaces, is possible. We determine the strength of subband mixing at an interface necessary to produce structure in the resonant-tunneling current. The second mechanism does not occur in normal resonant tunneling because the lateral wave vector is conserved during tunneling. Subband mixing produces two sets of fine structure. The first set appears for any contact-subband filling. The second set of peaks, which alternate with the first set of peaks, appears when two or more subbands are occupied. The results are used to better understand the recent observation of QBRT.

I. INTRODUCTION

With the recent advances in the art of microfabrication, zero-dimensional quantum structures can now be made which should exhibit quantum carrier confinement in all three dimensions. The effects of three-dimensional confinement in microcrystallites[1-5] have been observed by use of exciton luminescence. However, exciton luminescence of nanostructures made by laterally confining motion in two-dimensional semiconductor quantum wells (quantum boxes[6-11]) does not yet provide conclusive evidence for three-dimensional confinement in quantum-box structures.

Recently, Reed *et al.*[12] investigated electronic transport through a three-dimensionally confined quantum well to provide another characterization of the quantum box that might reveal the three-dimensional confinement effects more conclusively. The structure (see Fig. 1) was fabricated from a multilayer quantum-well structure containing n^+-type GaAs layers for contacts, $Al_xGa_{1-x}As$ barriers, and an $In_xGa_{1-x}As$ quantum well. Electron-beam lithography and reactive-ion etching were used to define isolated 0.1-μm-wide columns. Lateral motion was confined in the contacts, barriers, and quantum well. Reed *et al.* developed a procedure to contact the top of a single isolated column and they measured the resonant-tunneling (RT) current through the quantum box. Reed *et al.* investigated a structure which had an $n=1$ quantum-well resonance near the GaAs conduction-band edge and an excited state ($n=2$) resonance near the top of the $Al_xGa_{1-x}As$ barrier. Resonant tunneling through the $n=2$ quantum-well resonance was observed. At high temperature, the current-voltage characteristics are similar to the current-voltage characteristics for normal RT through two-dimensional wells and barriers. At low temperature ($T\sim 1.0$ K), additional fine structure was observed to be superimposed on the normal RT characteristics [see Fig. 1(b)]. The lowest two fine-structure peaks were split by an applied bias of 80 meV. Other peaks were split by 50 meV. Estimates made for the lateral confinement in the box due to the sidewall depletion suggested that confinement splits the states in the box by 25 meV, which is consistent with the 50-meV splitting of the RT peaks. As a consequence, Reed *et al.* concluded that the fine structure corresponds to the discrete density of states in the zero-dimensional quantum box. In this paper we will investigate theoretically two mechanisms to help understand the fine structure observed in quantum-box resonant tunneling (QBRT).

In a normal double-barrier resonant-tunneling structure that is formed from two-dimensional barriers and wells, the lateral motion (parallel to the interfaces) of the tunneling electron is described by a plane-wave eigenstate with wave vector $k_\perp$. The wave vector $k_\perp$ is conserved as the electron tunnels through the double-barrier structure, unless some extrinsic scattering mechanism is present. Thus each tunneling electron remains in a single channel and mixing of channels is not possible. Since the density of lateral states is continuous, no fine structure appears in the normal double-barrier RT current.

QBRT differs from normal RT in two important respects: first, the density of lateral states is discrete in QBRT; second, there is no analog to the conservation of momentum rule. If the lateral-confinement potential is different for different regions (contacts, barriers, and box), then the laterally quantized states will have different energies and wave functions in the different regions. A lateral state in one region can couple to a lateral state in the adjacent region if the overlap between the states is nonzero. An electron initially in a specific source-contact subband can tunnel through any box subband which couples to the contact subband due to wave-function mixing at the interfaces. The tunneling is a multichannel process.

In this paper we will determine whether either of these two differences between QBRT and normal RT can explain the fine structure observed in QBRT. One might expect to see fine structure just because the states are discrete. However, if the lateral confinement is the same throughout the structure (i.e., the contacts, barriers, and well densities of lateral states are the same), then one applied bias voltage will align all of the subband states in the well with the corresponding subbands in the contact. Slight shifts in the RT for each subband would occur because different sets of states contribute to the RT of subbands with different lateral-confinement energies. However, Chou *et al.*[13] calculated the QBRT when confinement is the same in each region and found that RT peaks due to different subbands are not resolvable. When the lateral confinement is different in different regions, the same applied bias will not align every well state with the corresponding contact subband. We will determine whether the discreteness of the density of states can provide RT fine structure when lateral confinement is different in each region.

Multichannel tunneling is also possible when lateral confinement is different in each region. Even when only one source-contact subband is occupied, multichannel tunneling through other subbands in the quantum box will produce fine structure in the QBRT. In this paper we will determine how strong the subband mixing at an interface must be to produce structure in the QBRT current.

Our results will show that having discrete states in the quantum box is not sufficient to produce fine structure in the QBRT if the lateral confinement is the same in all regions. The lateral confinement must be different in different regions for fine structure to be observed. In Sec. II we will present the model we use for the nanostructure investigated by Reed *et al.*[12] to observe QBRT. We will explain why the lateral confinement is expected to be different for different regions of that structure. In Sec. III we will briefly describe the calculation of multichannel transmission probabilities and RT currents when subband mixing at an interface must be included. Results and conclusions will be presented in Secs. IV and V.

II. MODELING THE QUANTUM-BOX NANOSTRUCTURE

The nanostructure investigated by Reed *et al.* is shown in Fig. 1. The post contains 0.5-μm-wide n^+-type GaAs layers for contacts, 4-nm $Al_{0.25}Ga_{0.75}As$ barriers, and a 5-nm $In_{0.08}Ga_{0.92}As$ quantum well. After etching, the post radius is 0.05 μm. We model motion along the post (z direction) by use of the effective-mass approximation with barrier and well potentials determined by the conduction-band offsets. Specifically, we use for effective masses the following, $m_{GaAs}=0.067m_e$, $m_{Al\text{-}Ga\text{-}As}=0.087m_e$, and $m_{In\text{-}Ga\text{-}As}=0.063m_e$; and for conduction-band offsets, $V_{GaAs}=0$, $V_{Al\text{-}Ga\text{-}As}=0.203$ eV, and $V_{In\text{-}Ga\text{-}As}=-0.072$ eV. For this choice of material parameters, we use a 6-nm $In_xGa_{1-x}As$ well (slightly larger than the well used by Reed *et al.*) so that we obtain two quantum-well resonances, the ground state ($n=1$) near the GaAs band edge and the $n=2$ resonance near the top of the barrier, as observed by Reed *et al.*

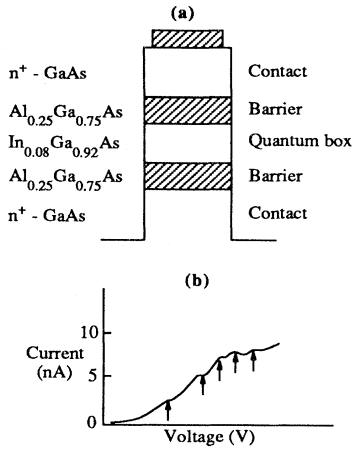

FIG. 1. (a) Schematic of the nanostructure used to observe quantum-box resonant tunneling. (b) Low-temperature ($T\sim 1.0$ K) current-voltage characteristics of an isolated quantum-box nanostructure. Tunneling occurs through the $n=2$ quantum-well resonance.

Reed *et al.* estimated a minimum width 13 nm for the (circular) flat-band conduction-path core in the quantum box; this estimate implies that the sidewall-depletion depth in the box is $\sim$43 nm. Since the flat-band core is small, the sidewall-depletion potential should be approximately parabolic everywhere in the box. For a parabolic potential with a Fermi-level pinning of $\Phi_T=0.7$ eV and box radius $R=50$ nm, Reed *et al.* estimated that the box-subband splitting is

$$\hbar\omega_{box}\approx(2\Phi_T/m_{In\text{-}Ga\text{-}As})^{1/2}\hbar R \approx 26 \text{ meV} .$$

The barriers and the well are undoped and should have similar sidewall-depletion depths. If the barrier has the same sidewall-depletion potential as the box, then $\hbar\omega_{barrier}$ scales as $(m_{barrier}/m_{box})^{1/2}$ and $\hbar\omega_{barrier}\approx 22$ meV. If the GaAs contacts had the same sidewall-depletion depth, then $\hbar\omega_{contact}$ would scale as $(m_{contact}/m_{box})^{1/2}$ and $\hbar\omega_{contact}\approx 25$ meV. However, the contacts are doped while barriers and well are undoped. The depletion depth should be shorter in the GaAs con-

tacts. For example, the depletion depth W in GaAs doped at 2×10^{18} cm^{-3} is about 22 nm.[12] Thus, the flat-band conduction-path core in the GaAs contact could be much wider than 13 nm and confinement effects could be weaker in the contact than in the box. A depletion depth as short as 22 nm implies a flat-band conduction-path core which is 56 nm wide. An infinite square well 56 nm wide would have a level splitting $\hbar\omega_{\text{contact}}$ of about 1–2 meV. We expect similar level splittings in the GaAs contacts.

An accurate model for the nanostructure would require accurate solution of the sidewall-depletion problem. Because the intent of this paper is to model QBRT rather than sidewall depletion, we have adopted the following simplified model for lateral confinement based on the estimates previously mentioned. The lateral-confining potentials are assumed to be parabolic and centered on the post axis. Thus, lateral wave functions (x and y directions) are harmonic-oscillator states and the energy levels are equally spaced. In the box, $\hbar\omega_{\text{box}}\approx26$ meV, and in the barrier, $\hbar\omega_{\text{barrier}}\approx22$ meV. Two extreme choices are possible for the contacts: either the contact has a similar depletion potential and $\hbar\omega_{\text{contact}}\approx25$ meV, or the depletion depth is much shallower and $\hbar\omega_{\text{contact}}\approx1$ meV. We will test both choices to determine which conditions produce RT fine structure. In either case the sidewall-depletion potential in the contact is not likely to be exactly parabolic. We use harmonic-oscillator states and equally spaced levels as a matter of convenience. The results we present will not be affected qualitatively by how we model the confinement.

III. CALCULATION OF MULTICHANNEL QUANTUM-BOX RESONANT TUNNELING

The theory of resonant tunneling through a single channel,[14] used to model normal RT, has been generalized to study multichannel tunneling in a confined quantum nanostructure. We assume that for each region in the structure the Hamiltonian can be separated into transverse (x and y directions) and parallel (z) parts,

$$H^i=H^i_\perp(x,y)+H^i_\parallel(z)\ , \tag{1}$$

where i indicates the region. In the effective-mass approximation

$$H^i_\perp(x,y)=-\frac{\hbar^2}{2m_i}\left[\frac{d^2}{dx^2}+\frac{d^2}{dy^2}\right]+V^i_{\text{conf}}(x,y)\ , \tag{2a}$$

$$H^i_\parallel(z)=-\frac{\hbar^2}{2m_i}\left[\frac{d^2}{dz^2}\right]+V_i+U_i(z)\ , \tag{2b}$$

where m_i is the effective mass, taken to be isotropic, V_i is the conduction-band offset (relative to the GaAs band edge), U_i is the applied bias potential, and V^i_{conf} is the confining potential. In our model,

$$V^i_{\text{conf}}(x,y)=\tfrac{1}{2}m_i\omega_i^2(x^2+y^2)\ , \tag{2c}$$

where $\hbar\omega_i$ is the subband splitting due to confinement.

Eigenstates for $H^i_\perp$ and $H^i_\parallel$ can be found:

$$H^i_\perp\phi_{in}(x,y)=E_{in}\phi_{in}(x,y)\ , \tag{3a}$$

$$H^i_\parallel f_{im}(z)=F_{im}f_{im}(z)\ . \tag{3b}$$

Then the total wave function in region i is

$$\Psi_i=\sum_{n,m}M^i_{nm}f_{im}\phi_{in}\delta(E-E_{in}-F_{im})\ , \tag{4a}$$

where

$$H^i\Psi_i=E\Psi_i\ . \tag{4b}$$

The boundary conditions at the interface ($z=z_0$) between layers i and $i+1$ are

$$\Psi_i(x,y,z_0)=\Psi_{i+1}(x,y,z_0)\ , \tag{5a}$$

$$\frac{1}{m_i}\frac{d}{dz}\Psi_i(x,y,z)\bigg|_{z=z_0}=\frac{1}{m_{i+1}}\frac{d}{dz}\Psi_{i+1}(x,y,z)\bigg|_{z=z_0}\ . \tag{5b}$$

Evaluating the boundary conditions, we obtain

$$\sum_m C^{i+1}_{nm}(z_0)=\sum_{p,q}C^i_{qp}(z_0)\langle i+1,n\,|\,i,q\rangle\ , \tag{6a}$$

$$\sum_m\frac{V^{i+1}_{nm}(z_0)}{m_{i+1}}=\sum_{p,q}\frac{V^i_{qp}(z_0)}{m_i}\langle i+1,n\,|\,i,q\rangle\ , \tag{6b}$$

with

$$C^i_{nm}(z_0)=f_{im}(z_0)M^i_{nm}\delta(E-E_{in}-F_{im})\ , \tag{6c}$$

$$V^i_{nm}(z_0)=\frac{dC^i_{nm}}{dz}\bigg|_{z=z_0}\ , \tag{6d}$$

and

$$\langle j,m\,|\,i,q\rangle=\int dx\int dy\,\phi^*_{jm}\phi_{iq}\ . \tag{6e}$$

If confinement is the same on both sides of the interface, then $\langle i+1,m\,|\,i,q\rangle=\delta_{m,q}$ and tunneling is a single-channel process. When the confinement is different in two adjacent regions, then subband mixing at the interface is possible.

The applied bias potential in Eq. (2b) is assumed to vary linearly in each region. The wave functions f_{im} are found by solving Eq. (3b). The linear bias potential is approximated by a set of step functions and Eq. (3b) is solved numerically. Two solutions exist for each energy F_{im} corresponding to waves propagating in opposite directions. By use of the f_{im} to evaluate Eqs. (6c) and (6d), and Eqs. (6a) and (6b) to match wave functions at an interface, one obtains a matrix equation connecting the M^i_{nm} of the source contact with the M^i_{nm} for the drain contact. Let F_{im} ($m>0$) correspond to solutions propagating from source to drain, and F_{im} ($m<0$) correspond to solutions propagating in the reverse direction. The matrix equation connecting M^s_{nm} and M^d_{nm}, in which s and d refer to source and drain, is solved by assuming that the tunneling electron incident on the source-contact barrier is in a single state $M^s_{nm}=\delta_{m,m_0}\delta_{n,n_0}$ if $m>0$, and by requiring that $M^d_{nm}=0$ if $m<0$. The reflected particle current due to an incident electron with energy E, wave

vector k_0, and lateral state n_0 is

$$S_r(E,n_0)=\sum_{p,m<0}{}' \frac{\hbar k_m}{m_s}|M^s_{pm}|^2 , \tag{7}$$

where the sum is restricted to states with $E_{sp}+F_{sm}=E$, where m_s and m_d are the effective masses in each region, and k_m is the wave vector of state f_{sm}. The transmitted particle current is

$$S_t(E,n_0)=\sum_{r,m>0}{}' \frac{\hbar k_m}{m_d}|M^d_{rm}|^2 , \tag{8}$$

with $E_{dr}+F_{dm}=E$. Probability density is conserved, so

$$S_t(E,n_0)=\frac{\hbar k_0}{m_s}+S_r(E,n_0) .$$

The total RT current is

$$J_{\rm tot}=\frac{e}{\pi\hbar}\sum_n \int_{E_{sn}} dE \frac{S_t(E,n)m_s}{\hbar k}[f_s(E)-f_d(E)] , \tag{9}$$

where $f_{s,d}$ are the source and drain Fermi functions, $f_d(E)=f_s(E+U)$, U is the applied bias, k is the wave vector for an incident electron in subband n with energy E, and the sum is over occupied source-contact subbands.

In our calculations we evaluate $J_{\rm tot}$ at zero temperature. The number of occupied contact subbands is determined by the Fermi energy E_F. E_F is related to the charge density ρ in the source contact by ($T=0$)

$$\rho=\frac{1}{A\pi}\sum_{\substack{n\\(E_{sn}<E_F)}}\left[\frac{2m_s(E_F-E_{sn})}{\hbar^2}\right]^{1/2} , \tag{10}$$

where A is the cross-sectional area of the contact ($A=\pi R^2$, $R\sim 0.05$ μm for the structure of Reed *et al.*).

The strength of the coupling of different channels is determined by the overlap between lateral states of different regions. If we make the approximation that the confining potentials are parabolic [Eq. (2c)], then the overlaps can be determined analytically. Even if the confining potential is not exactly parabolic, the parabolic approximation should give a good qualitative estimate of the overlaps if the correct effective mass and level spacing $\hbar\omega$ are used to model the parabolic potential.

The one-dimensional harmonic-oscillator state with energy $\hbar\omega(n+\frac{1}{2})$ is

$$\phi_{n,\alpha}(x)=N_n H_n(\alpha x)e^{-\alpha^2x^2/2} , \tag{11}$$

where H_n is the Hermite polynomial, N_n is the normalization factor, and $\alpha=(m\hbar\omega)^{1/2}/\hbar$. The overlap $\langle i,n|j,m\rangle$ [Eq. (6e)] is a function of $\xi=\alpha_j/\alpha_i$. Specifically

$$\langle i,n|j,m\rangle=0 \quad \text{if } n+m \text{ is odd} ,$$

$$\langle i,n|j,m\rangle=\left[\frac{2\xi n!m!}{(1+\xi^2)^{n+m+1}}\right]^{1/2} I, \quad I=\sum_{\substack{p=0,2,\ldots \text{ if } n \text{ even}\\ p=1,2,\ldots \text{ if } n \text{ odd}}}^{\min(n,m)} \frac{2^p\left[\frac{1-\xi^2}{2}\right]^{(n-p)/2}\left[\frac{\xi^2-1}{2}\right]^{(m-p)/2}\xi^p}{\left[\frac{n-p}{2}\right]!\left[\frac{m-p}{2}\right]!p!} .$$

For example, if $n=m=0$, then

$$\langle i,0|j,0\rangle=\left[\frac{2\xi}{1+\xi^2}\right]^{1/2}$$

(see Fig. 2). Using the level splittings and effective masses for $Al_xGa_{1-x}As$ and $In_yGa_{1-y}As$, $\alpha_{\text{Al-Ga-As}}/\alpha_{\text{In-Ga-As}}=1.08$. Level mixing at $Al_xGa_{1-x}As/In_yGa_{1-y}As$ interfaces should be very weak. If the confinement in GaAs is similar to the confinement in $In_xGa_{1-x}As$, then $\hbar\omega_{\text{GaAs}}\approx 25$ meV and $\alpha_{\text{Al-Ga-As}}/\alpha_{\text{GaAs}}=1.07$. However, if the confinement is much weaker in GaAs and $\hbar\omega_{\text{GaAs}}\approx 1$ meV, then $\alpha_{\text{Al-Ga-As}}/\alpha_{\text{GaAs}}=5.34$. In the latter case $\langle \text{GaAs},0|Al_xGa_{1-x}As,0\rangle\sim 0.6$ and level mixing should be significant.

The overlap matrix is unitary when all subbands are included. However, only a finite number of subbands are included in the multichannel problem, so that the matrix equations can be solved to determine the multichannel transmission probabilities. The overlap matrix for restricted sets of subbands, constructed using, for example, the harmonic-oscillator states, is not unitary because overlap with excluded states is not included. The transmission probabilities cannot be accurately determined when the overlap matrices are nonunitary. Thus, even for a restricted set of subbands, the overlap matrices must be made explicitly unitary.

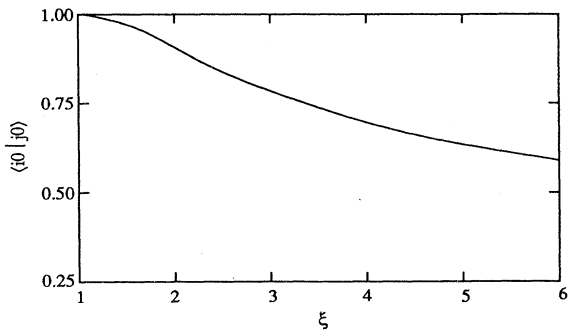

FIG. 2. Overlap between $n=0$ oscillator states as a function of ξ.

When the quantum nanostructure is cylindrically symmetric, as in the model with parabolic confining potentials, subbands in different regions can mix at the interface only if each subband has the same x (y) parity. Thus there are four sets of coupled channels. The subbands with even x parity and even y parity are coupled. These subbands couple to the lowest-energy subband in the contacts. Similarly, subbands with even (odd) x parity and odd (even) y parity are coupled and couple to the first-excited-state subbands in the contacts. Subbands with odd x parity and odd y parity are coupled and couple to one of the second-excited-state subbands in the contacts.

To obtain a qualitative understanding of the effects of subband mixing, we have considered the following model: for each type (x and y parity) of channel we include the lowest-energy subband of that type and the three higher-energy subbands which are formed from the ground state and first-excited oscillator states for x motion and for y motion with the appropriate parity. For example, for the channels with even x parity and even y parity (i.e., for harmonic-oscillator states $n_x=0,2,4,\ldots$ and $n_y=0,2,4,\ldots$) we include the subbands with $(n_x,n_y)=(0,0)$, (0,2), (2,0), and (2,2). The form of the overlap matrix between subbands which mix at an interface is determined by the unitarity requirement. For our simplified model the overlap matrix for x (y) motion is 2×2. A real, unitary 2×2 matrix has the form

$$\begin{bmatrix} \beta & \gamma \\ -\gamma & \beta \end{bmatrix},$$

where $|\gamma|=(1-\beta^2)^{1/2}$ (other choices for the signs of the matrix elements are possible by changing the signs of the basis functions). By specifying β_x and β_y for the x and y overlaps, the total overlap matrix for the four coupled subbands can be determined. We have performed calculations for the simplest case: $\beta_x=\beta_y=\beta$, with β the same for all channels.

IV. RESULTS

Calculations have been performed to determine (1) what conditions are necessary for lateral confinement effects to be significant, and (2) whether the discrete density of states or subband mixing can explain the QBRT fine structure. To answer, in part, the first question, we have performed calculations for nanostructures with similar lateral confinement in the box and contacts ($\hbar\omega_{\text{box}}\approx\hbar\omega_{\text{contact}}$) and with lateral confinement in the box very different (stronger) from confinement in the contacts ($\hbar\omega_{\text{box}}\gg\hbar\omega_{\text{contact}}$). We have performed calculations to investigate each of the two mechanisms. We have calculated the QBRT assuming that subbands do not couple (referred to as diagonal tunneling because the overlap matrices are diagonal). In diagonal tunneling, fine structure occurs because the density of states is discrete and the different channels have different subband energies. We also have calculated the QBRT by assuming that subband mixing at interfaces is important. The fine structure depends on the number of occupied contact subbands. Table I lists the cases we have considered; E_F and ρ are related by Eq. (10). We have performed calculations for one, two, three, and four occupied subbands when $\hbar\omega_{\text{contact}}\ll\hbar\omega_{\text{box}}$ and for one, two, and three occupied subbands when $\hbar\omega_{\text{contact}}\approx\hbar\omega_{\text{box}}$. All calculations were performed for $T=0$.

TABLE I. Subband filling in the contact. The contact-subband filling is determined by use of Eq. (10), assuming the post radius is 50 nm and $T=0$.

$\hbar\omega_{\text{contact}}$ (meV)	ρ (cm^{-3})	$E_F/\hbar\omega_{\text{contact}}$
1	1×10^{15}	1.35
	4×10^{15}	2.35
	1×10^{16}	3.42
	2×10^{16}	4.55
25	4×10^{15}	1.22
	2×10^{16}	2.35
	5×10^{16}	3.42

As mentioned, we have tested two models for the lateral quantization: $\hbar\omega_{\text{contact}}\approx\hbar\omega_{\text{box}}$ and $\hbar\omega_{\text{contact}}\ll\hbar\omega_{\text{box}}$. Two models for the applied bias potential have also been tested. In one model, equal potential drops occur across each barrier; there is no potential drop across the well. In the other model the potential drops across the well and across each barrier in proportion to the width of each region. The first-excited state of the quantum well (the state observed by Reed *et al.* in QBRT) is sharper in the first model for the potential drop than in the second model. Thus QBRT fine structure will be easier to resolve when the first model for the potential drop is used.

The effect of the discrete density of lateral states on QBRT is determined by calculating the RT in the diagonal-tunneling approximation so no effects of level mixing are included. Figure 3 shows the QBRT current-

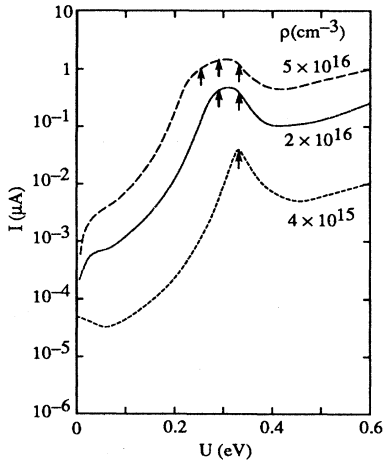

FIG. 3. QBRT current-voltage characteristics calculated in the diagonal tunneling approximation, with no potential drop in the well, and $\hbar\omega_{\text{box}}\approx\hbar\omega_{\text{contact}}$. Arrows indicate the peak positions of RT through the first-excited well state from each subband in the contact. The contact charge density is indicated.

voltage characteristics calculated in the diagonal-tunneling approximation with no potential drop in the well and with similar lateral confinement in the box and contacts ($\hbar\omega_{box} \approx \hbar\omega_{contact}$). Arrows indicate the peak positions of the RT through the first-excited ($n=2$) well state from each subband in the contact. Individual peaks are broad (see the RT for $\rho = 4\times10^{15}$ cm^{-3}, which involves only one subband) and cannot be resolved when more than one contact subband is occupied. Moreover, there is no evidence for tunneling through the well ground state ($n=1$). Chou *et al.*[13] also found that individual peaks were not resolvable. Since $\hbar\omega_{contact} \approx \hbar\omega_{box}$, the same applied voltage should line up all of the box subbands with the corresponding contact subbands. The small shifts (less than $2\hbar\omega_{box}$) in RT peaks for different subbands occur because a different distribution of states is occupied in each subband. However, these shifts are smaller than the width of the individual peaks. Similar results were obtained when the bias potential was modeled with a drop across the well.

When lateral confinement is much weaker in the contact than in the box ($\hbar\omega_{contact} \ll \hbar\omega_{box}$), the QBRT fine structure is clearly resolved (see Fig. 4). The RT through the first-excited state ($n=2$) can be resolved even though this state is not as sharp as the ground state. One peak appears for RT through each well state ($n=1,2,\ldots$) for each occupied contact subband. The fine structure is resolved when $\hbar\omega_{contact} \ll \hbar\omega_{box}$ since a different bias voltage is needed to line up each contact subband with the corresponding box subband. Adjacent RT peaks are separated by a bias of about $2\hbar\omega_{box}$. All of the contact subbands have nearly the same energy (relative to the much larger box-subband energies); therefore, the separation in RT fine-structure peaks is determined by the energy separation of the box subbands. When the bias voltage is modeled with a drop in the well, the $n=2$ peaks cannot be resolved.

The effects of subband mixing at the contact-barrier interface on the QBRT current-voltage characteristics are shown in Figs. 5–7. The subband mixing at the contact-barrier interface is described by use of the simple model discussed in the preceding section. Subband mixing at the barrier-box interface is ignored because each region has similar lateral confinement. Figure 5 shows the RT when $\beta_x = \beta_y = 0.8$ for even- and odd-parity states and the lateral confinement in the contact is much weaker than the box lateral confinement. When only the lowest-energy contact subband is occupied, RT fine-structure peaks appear for tunneling from the ground-state contact subband through each well subband with even x parity and even y parity, not just for tunneling through the lowest box subband as occurs in diagonal tunneling. The peaks are separated by $4\hbar\omega_{box}$ because the even-parity subbands are separated by $2\hbar\omega_{box}$. When the second contact subband [even x (y) parity and odd y (x) parity] is occupied, an additional set of RT peaks appears. These peaks are also separated by $4\hbar\omega_{box}$, but the peaks are shifted by $2\hbar\omega_{box}$ from the set of peaks due to tunneling from the ground-state contact subband. No additional peaks occur when more than two subbands are occupied because the RT peaks for higher-energy contact subbands occur at the same bias voltages as the RT peaks for the two lowest-energy subbands.

The peaks are clearly resolved in Fig. 5 for both $n=1$ and 2 well states. When the applied potential is modeled with a voltage drop in the well, the $n=2$ RT fine structure is more difficult to resolve when several contact subbands are occupied. When the box and contact lateral confinement are similar ($\hbar\omega_{box} \approx \hbar\omega_{contact}$), the $n=2$ peaks cannot be resolved if more than one contact subband is occupied.

We have also calculated QBRT when the subband mix-

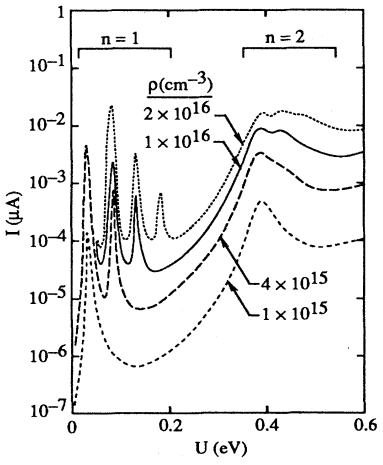

FIG. 4. QBRT current-voltage characteristics calculated in the diagonal tunneling approximation, with no potential drop in the well, and $\hbar\omega_{box} \gg \hbar\omega_{contact}$. Tunneling through the ground state ($n=1$) and first-excited state ($n=2$) in the well are indicated.

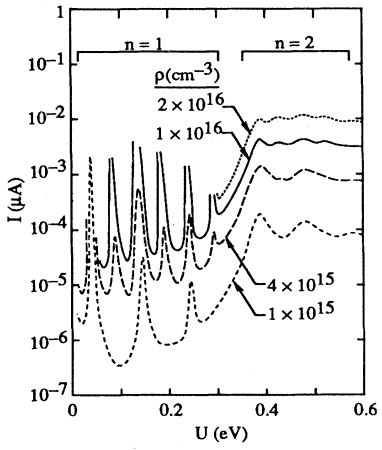

FIG. 5. QBRT current-voltage characteristic calculated with subband mixing ($\beta=0.8$), with no potential drop in the well and $\hbar\omega_{box} \gg \hbar\omega_{contact}$.

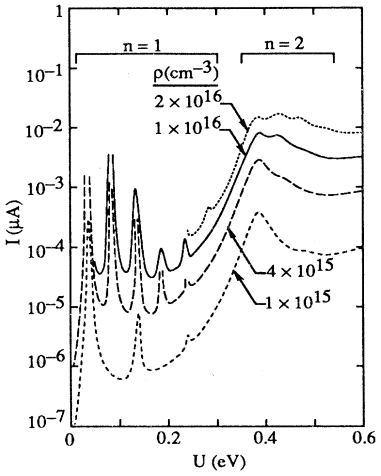

FIG. 6. QBRT current-voltage characteristic calculated with subband mixing ($\beta=0.98$), with no potential drop in the well and $\hbar\omega_{\text{box}} \gg \hbar\omega_{\text{contact}}$.

ing is possible but weak ($\beta_x=\beta_y=0.98$ for each channel). Fine structure due to subband mixing is present for both the $n=1$ and 2 well states (see Fig. 6), even for weak coupling. However, when more than one contact subband is occupied, additional fine structure in the $n=2$ peak due to the subband mixing is difficult to identify (compare Figs. 4 and 6). Structure in the $n=1$ peak due to weak subband mixing is easy to identify even when four contact subbands are occupied.

The QBRT fine structure for the $n=2$ peak is shown in Fig. 7 as a function of the subband coupling. The current-voltage characteristics are shown for a structure with weak contact confinement ($\hbar\omega_{\text{contact}} \ll \hbar\omega_{\text{box}}$) and with three occupied contact subbands ($\rho=1\times10^{16}$ cm^{-3}). The resolution of RT peaks for $\beta=0.98$ and 0.8 is clearer in Fig. 7 than in Figs. 5 and 6 because a linear, rather than logarithmic, scale is used in Fig. 7. The magnitudes of the current ($I\sim1-10$ nA) is consistent with the currents observed by Reed *et al.* In fact, a comparison of Figs. 3–6 shows that the magnitudes of the

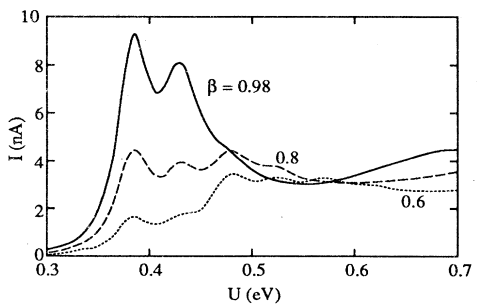

FIG. 7. QBRT current-voltage characteristic calculated with subband mixing ($\beta=0.98$, 0.8, and 0.6), with no potential drop in the well, $\hbar\omega_{\text{box}} \gg \hbar\omega_{\text{contact}}$, and $\rho=1\times10^{16}$ cm^{-3}.

current are consistent with the results of Reed *et al.*, except when $\hbar\omega_{\text{contact}} \approx \hbar\omega_{\text{box}}$; in that case, the currents are too large.

Two features of the RT fine structure depend on the strength of subband coupling and have direct relevance to the results of Reed *et al.* For weak coupling, only the RT fine-structure peaks at low bias are important. As the coupling increases, peaks for RT through higher-energy box subbands become just as important. The peaks at higher bias have the larger magnitude when $\beta=0.6$. In the experiment of Reed *et al.*, the fourth fine-structure peak (see Fig. 1) for RT in the $n=2$ state has the largest magnitude. Because the fine-structure peaks at high bias are observable, the subband mixing should be significant.

Reed *et al.* also observed a difference in bias voltage between the first two fine-structure peaks that was roughly twice the difference between other peaks. The box confining potential does have a flat-band core region. A state localized in this region should experience less confinement than if the parabolic confining potential extended through the core. Thus the energy spacing between the ground state and the first-excited state could be larger than predicted by a parabolic confining potential that has been modeled to provide the correct spacing for the higher subbands. A wide separation between RT peaks might also occur if the lower of the two peaks were a fine-structure peak for tunneling through the $n=1$ well state. However, the large separation between the first two peaks can also be explained when subband mixing is large. As shown in Fig. 7, the second fine-structure peak is small compared to the first two large peaks, which are due to tunneling in the channels coupled to the ground-state subband. The second peak might be missing if any additional broadening were present. Thus, two features of the observed QBRT fine structure, the missing peak and the higher currents at peaks for tunneling through higher-energy subbands, are consistent with having large subband coupling during the resonant tunneling.

V. CONCLUSIONS

Calculations of quantum-box resonant tunneling have been performed to determine what conditions are necessary to observe lateral-quantization effects in QBRT and to determine how different mechanisms reveal the lateral-quantization effects. A phenomenological model has been used to investigate QBRT because modeling QBRT accurately is a complicated problem. The model is too simple to provide quantitative results. However, the results do identify qualitatively the conditions necessary for lateral quantization to affect QBRT. One necessary condition which can be identified is that lateral confinement in the box should be different from lateral confinement in the contact. When contact and box subbands have similar energy spacings, these peaks are difficult to resolve.

Two intrinsic mechanisms have been investigated to determine how they reveal the lateral-quantization effects. The discrete density of lateral states (diagonal tunneling) produces fine structure in the QBRT: one

fine-structure peak occurs for each occupied contact subband for each well state that is a channel for resonant tunneling. When $\hbar\omega_{box} >> \hbar\omega_{contact}$, the fine-structure peaks for tunneling through a particular well state are separated by a voltage of $2\hbar\omega_{box}$.

When subband mixing at the contact-barrier interface is important, two sets of QBRT fine-structure peaks can appear. The first set of peaks results from tunneling that involves channels which couple to the contact ground-state subband. Those fine-structure peaks in the first set which are for tunneling through a particular well state are separated by a bias of about $4\hbar\omega_{box}$ when $\hbar\omega_{box} >> \hbar\omega_{contact}$. The second set of peaks, shifted from the first set by a bias of $2\hbar\omega_{box}$, appears when more than one contact subband is occupied. These peaks correspond to tunneling which involves channels that couple to the first-excited subbands in the contact. Tunneling from other contact subbands exhibits RT peaks which occur at the same biases as the first two sets of peaks. The missing peak and relative intensities of fine-structure peaks observed by Reed *et al.* can be explained if subband coupling at the contact-barrier interface is large.

Subband coupling appears to provide a more consistent explanation of the observed QBRT fine structure. However, the dependence of the fine structure on contact-subband filling is very different for the two mechanisms. A study of QBRT as a function of subband filling should identify the importance of each mechanism.

Our results provide qualitative insight on lateral quantization effects in QBRT. The current-voltage characteristics of QBRT are extremely sensitive to the model used to describe the potential drop in the well, the model used to describe lateral confinement in each region, and the band filling. Accurate three-dimensional modeling of the charge depletion at the interfaces and near the sidewalls will be necessary to treat accurately the effects of lateral confinement, the state filling, and the potential profile on QBRT.

ACKNOWLEDGMENTS

This work was performed under the McDonnell Douglas Corporation Independent Research and Development Program. The author would like to thank M. Reed for several enlightening discussions about his experimental results.

[1]L. Brus, IEEE J. Quantum Electron. **QE-22**, 1909 (1986), and references therein.

[2]C. J. Sandroff, D. M. Hwang, and W. M. Chung, Phys. Rev. B **33**, 5953 (1986).

[3]J. Warnock and D. D. Awschalom, Appl. Phys. Lett. **48**, 425 (1986).

[4]A. I. Ekimov, A. A. Onushchenko, M. É. Raikh, and Al. L. Éfros, Zh. Eksp. Teor. Fiz. **90**, 1795 (1986) [Sov. Phys.—JETP **63**, 1054 (1986)].

[5]A. I. Ekimov, A. A. Onushchenko, S. K. Shumilov, and Al. L. Éfros, Pis'ma Zh. Tekh. Fiz. **13**, 281 (1987) [Sov. Tech. Phys. Lett. **13**, 115 (1987)].

[6]P. M. Petroff, J. Cibert, A. C. Gossard, G. J. Dolan, and C. W. Tu, J. Vac. Sci. Technol. B **5**, 1204 (1987).

[7]J. Cibert, P. M. Petroff, G. J. Dolan, S. J. Pearton, A. C. Gossard, and J. H. English, Appl. Phys. Lett. **49**, 1275 (1986).

[8]H. Temkin, G. J. Dolan, M. B. Panish, and S. N. G. Chu, Appl. Phys. Lett. **50**, 413 (1987).

[9]K. Kash, A. Scherer, J. M. Worlock, H. G. Craighead, and M. C. Tamargo, Appl. Phys. Lett. **49**, 1043 (1986).

[10]M. A. Reed, R. T. Bate, K. Bradshaw, W. M. Duncan, W. R. Frensley, J. W. Lee, and H. D. Shih, J. Vac. Sci. Technol. B **4**, 358 (1986).

[11]Y. Miyamoto, M. Cao, Y. Shingai, K. Furuya, Y. Suematsu, K. G. Ravikumar, and S. Arai, Jpn. J. Appl. Phys. **26**, L225 (1987).

[12]M. A. Reed, J. N. Randall, R. J. Aggarwal, R. J. Matyi, T. M. Moore, and A. E. Wetsel, Phys. Rev. Lett. **60**, 535 (1988).

[13]S. Y. Chou, E. Wolak, and J. S. Harris, Jr., Appl. Phys. Lett. **52**, 657 (1988).

[14]See, for example, M. O. Vassell, J. Lee, and H. F. Lockwood, J. Appl. Phys. **54**, 5206 (1983).